Yongfeng Qi, Jing Li*, Chengbin Shi and Qintian Zhu

Continuous Cooling Transformation of Undeformed and Deformed High Strength Crack-Arrest Steel Plates for Large Container Ships

https://doi.org/10.1515/htmp-2018-0003
Received January 05, 2018; accepted June 03, 2018

Abstract: The phase transformation behavior of crack-arrest steel during continuous cooling either with or without deformation at high temperatures was investigated. By carefully examining the microstructures of continuous cooled samples, we found that pearlite, quasi-polygonal ferrite (QPF), acicular ferrite (AF), granular bainite (GB), upper bainite, lath-like bainite and martensite/austenite will exist depending on cooling rates and transformation temperatures in both conditions of deformation and without deformation after austenization. The transformation curves of AF and GB moved toward the left in deformation condition in comparison with that of without deformation condition, which indicated that deformation promoted the formation of QPF and AF; meanwhile, deformation inhibited the formation of bainite. Finer bainite and the accompanying M/A could be obtained by reducing the bainite nucleation activation energy as follows: (i) increasing the undercooling by increasing the cooling rate; (ii) increasing the stored energy by deformation of the austenite.

Keywords: continuous cooling transformation, container ship, microstructure, cooling rate, deformation

Introduction

With the growth of world economy and transportation volume, the need for building large container ships has been expanded for the purpose of reducing cost and improving transportation efficiency. Dead weight has a major influence on transportation efficiency so that weight saving is a key factor for building large container ships [1]. To reduce the plate thickness, more advanced plates with high strength and good toughness are required.

In recent years, the 60 mm thick plates with 460 MPa yields strength class have been developed by JFE steel to replace conventional 80 mm plates for energy conservation. The thermo-mechanically controlled process (TMCP) technology combined with accelerated cooling as an effective method for microstructure control during production of steels has been widely employed to achieve high strength steel plates used in large container ships [2,3]. This imposes a requirement for shipbuilding steel to develop optimal microstructure, which should offer the potential for improving the strength and toughness. Steels that are hot rolled and cooled to exhibited high strength and good toughness often require acicular ferrite (AF) and bainite microstructure [4]. Developing optimal microstructure is not an independent factor, which is related to chemical composition, hot deformation processing and accelerated cooling rate. Some alloy elements, such as aluminum, chromium, niobium, copper, titanium and molybdenum, are often added to achieve the satisfied microstructure and accordingly improve the strength and toughness [5–7]. During the process of alloy design, carbon equivalent (C_{eq}) and cold cracking susceptibility (P_{cm}) should be considered, in which the two parameters are calculated by eqs. (1) and (2) [8, 9] so that optimal balance between the properties of the base plate and welded joint could be achieved.

$$C_{eq} = C + (Mn + Si)/6 + (Cu + Ni)/15 + (Cr + Mo + V)/5 \quad (1)$$

$$P_{cm} = C + Si/30 + (Mn + Cu + Cr)/20 + Mo/15 + V/10 + Ni/60 + 5B \quad (2)$$

The main factors to control TMCP are hot deformation strain, hot deformation temperature and subsequently cooling rate. These parameters are essential in controlling microstructure formation based on phase transformation theory. In engineering application, a continuous cooling transformation (CCT) diagram is powerful to display the phase transformation behavior in TMCP

***Corresponding author: Jing Li,** State Key Laboratory of Advanced Metallurgy, University of Science and Technology Beijing (USTB), Beijing, P. R. China, E-mail: lijing@ustb.edu.cn
Yongfeng Qi: E-mail: yongfeng_qi@126.com, **Chengbin Shi:** E-mail: chengbin.shi@ustb.edu.cn, **Qintian Zhu:** E-mail: zqtustb@163.com, State Key Laboratory of Advanced Metallurgy, University of Science and Technology Beijing (USTB), Beijing, P. R. China

processing which can also be used to predict the constitution of microstructure.

In this work, the phase transformation of low-carbon high strength steel used as shipbuilding plate was investigated in the non-deformed and deformed conditions. The object is to clarify the rule of AF and bainite formation by investigating the effects of hot deformation and deformation temperature on the behavior of phase transformation, then plot the CCT curves in two different conditions. It would be beneficial to practical application of TMCP processing to product high performance shipbuilding steels.

Experimental procedure

The chemical compositions of the experimental materials cut from an industrial hot rolled sheet are shown in Table 1. The value of C_{eq} and P_{cm} is 0.47 and 0.208, respectively. Samples were prepared as ϕ8 mm × 80 mm with effective testing length of 15 mm in the center region to carry out thermomechanical simulation tests under undeformed and deformed conditions.

The thermomechanical experiments were conducted on a Gleeble 3800 thermomechanical simulator (Dynamic System Inc., Poestenkill, NY) in order to plot static (without hot deformation) CCT diagrams and the dynamic (with hot deformation) CCT diagrams. The critical temperature for deformation within austenite phase region is T_{95} (completely recrystallized temperature) and T_5 (recrystallization-stop temperature) [10]. Deformation above T_{95} leads to complete recrystallization of austenite, which is also accompanied with grain refinement at the same time. Deformation below T_5 results in high densities of substructure and dislocation, which increases the nucleation sites of AF and bainite, and it is regarded as a desirable microstructure prior to final cooling. Deformation between T_{95} and T_5 leads to mixed grain and poor final microstructure and properties. Therefore, the temperature for deformation within the later region should be avoided. The critical temperature for deformation in dynamic CCT tests was T_{95}, 1,323 K (1,050°C), and T_5, 1,173 K (900°C), respectively, which were determined in a separate experiment for the steel used in these experiments [4]. The schematic diagram for the continuous cooling experiments are shown in Figure 1 and detailed experimental process are as follows:

(1) All specimens in static simulate experiments were first austenitized for 5 min at 1,200°C and then cooled to ambient temperature at the cooling rates of 0.1, 0.5, 2, 5, 10, 20, 30 and 40°C s^{-1}, respectively.
(2) All specimens in dynamic simulate experiments were first austenitized for 5 min at 1,200°C and subsequently deformed by approximately 40 % at 1,050°C and then cooled to ambient temperature at the cooling rates of 0.1, 0.5, 2, 5, 10, 20, 30 and 40°C s^{-1}, respectively.
(3) To investigate the effect of hot deformed temperature on microstructure transformation, deformation

Table 1: Chemical compositions of the tested steels (wt%).

C	Mn	Si	S	P	Al	Cu	Ni	Cr	Mo	Nb	Ti	Fe	C_{eq}	P_{eq}
0.054	1.51	0.14	0.002	0.004	0.034	0.99	0.98	0.16	< 0.005	0.24	0.0098	Bal.	0.47	0.208

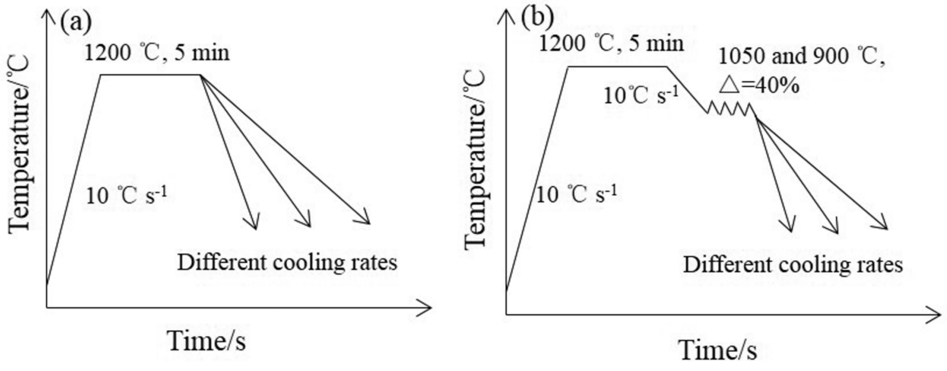

Figure 1: Schematic diagrams for the continuous cooling experiments: (a) Static simulation; (b) Dynamic simulation.

at 900°C was carried out to be compared with results in experiment 2. Three specimens were austenitized for 5 min at 1,200°C and subsequently deformed by approximately 40 % at 900°C and then cooled to ambient temperature at the cooling rates of 2, 10 and 40°C s^{-1}, respectively.

Specimens for metallographic examination were cut on wire cutting machine paralleled to the length direction at the center part. All the specimens were mechanically polished and etched with a 4 % Nital solution and then observed with an optical microscopy (LEICA DM2500M, OM) and scanning electron microscope (FEI MLA250, FEI, Hillsboro, OR, USA, SEM). Vickers microhardness measurement was employed on a THV-1MDX tester using a 200-g load and holding for 10 s. The microhardness was taken average of five points measurement in each specimen. Then, static and dynamic CCT curves were plotted based on the analyzing of measuring temperature, dilatation curves, microstructure and microhardness.

Results and discussion

Effects of cooling rates on transformation microstructures

Optical micrographs of the specimens under different cooling rates in the static and dynamic simulate tests are shown in Figures 2–4, respectively, which reveals the microstructure evolution with cooling rate increased from 0.1 to 40°C s^{-1}. Microstructure evolution in CCT specimens was almost composed of pearlite (P), quasi-polygonal ferrite (QPF), AF, granular bainite (GB), upper bainite (UB), lath-like bainite (LB) and corresponding martensite/austenite constitute (M/A island) depending on different cooling rates and transformation temperatures.

The microstructure metallographs in non-deformation condition were shown in Figure 2; it can be seen that QPF is the dominant component with a little P microstructure at the cooling rate of 0.1°C s^{-1}. When the cooling rate ranges from 0.5 to 2°C s^{-1}, QPF and AF become the principal components combined with the increase of AF percent, gradually. And corresponding microhardness increases from HV170 to HV207. UB and GB are initially formed at the cooling rate of 5°C s^{-1}. When the cooling rate is in the ranges of 5–20°C s^{-1}, UB and GB are majority phases, resulting in the microhardness increases to HV250. When the cooling rate ranges from 30 to 40°C s^{-1}, refined LB microstructure formed in prior austenite grain and the corresponding microhardness increased to HV270.

The microstructure metallographs in pre-deformation condition were shown in Figure 3; it can be seen that QPF is the dominant component with a little P microstructure at the cooling rate of 0.1°C s^{-1} and the corresponding microhardness is HV172. When the cooling rate ranges from 0.5 to 10°C s^{-1}, QPF and AF become the principal components combined with the increase of AF percent, gradually. And corresponding microhardness increases from HV216 to HV227. UB and GB are initially formed at the cooling rate of 20°C s^{-1}. When the cooling rate is in the ranges of 30–40°C s^{-1}, UB and GB are majority phases, resulting in the microhardness increases to HV275. In conclusion, hot deformation could enlarge the formation of AF and QPF from cooling rate of 0.5–2 to 0.5–20°C s^{-1}. Furthermore, the corresponding microstructure could be finer under hot deformation.

The microstructures of deformation at temperature 900°C are shown in Figure 4, with the cooling rates of 2, 10 and 40°C s^{-1}, respectively. The microstructure is mainly occupied by QPF at the cooling rate of 2°C s^{-1}, and the corresponding microhardness is HV205. With cooling rate increasing to 10°C s^{-1}, the microstructure transforms to AF and microhardness increases to HV255. When the cooling rate is 40°C s^{-1}, the microstructure consists of finer AF and GB. It can be seen that microstructure under the three cooling rates is finer compared with which deformed at 1,050°C.

In contrast, the corresponding CCT microstructure in the deformed conditions at a temperature of 1,050 and 900°C is obviously different in shape from those in the undeformed conditions due to hot deformation. Compared the microstructure of Figures 2 and 3 or 4, it can be seen that hot deformation could strongly promote the formation of AF and suppress the formation of GB and UB with the cooling rates ranging from 0.5 to 10°C s^{-1}. At the same time, the corresponding microstructure in deformed conditions is refined and LB cannot be found.

The CCT diagrams

The CCT diagrams are believed to be useful in gaining an insight into microstructure and designing an optimal TMCP during industrial processing of steels. The static and dynamic CCT diagrams of shipbuilding steel are shown in Figures 5(a) and (b), respectively, which exhibit multilayer transformation curves as cooling rate increased from 0.1 to 40°C s^{-1}. Solid points were

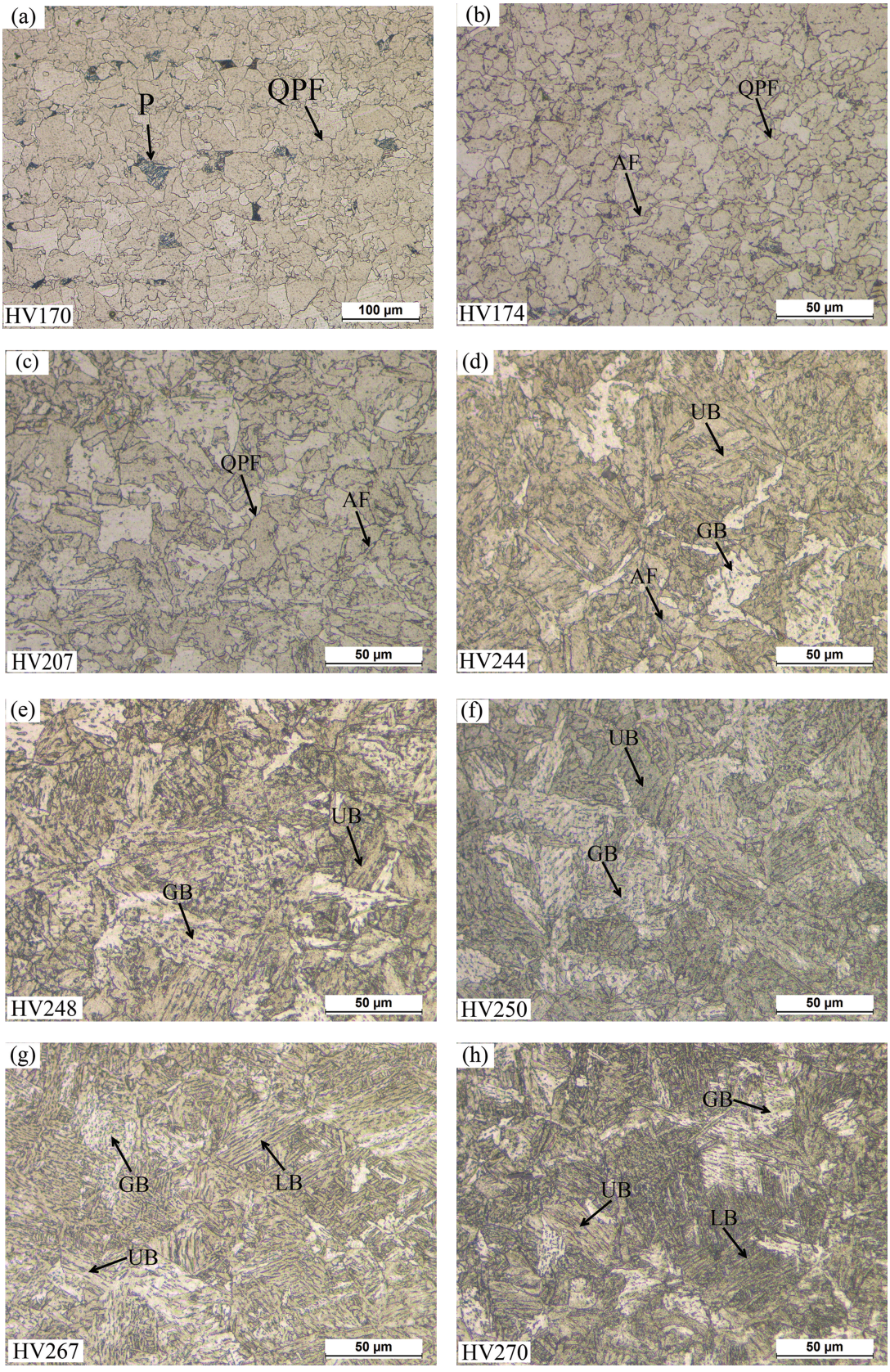

Figure 2: Optical microstructure of specimens at different cooling rates (static CCT): (a) 0.1 °C s^{-1}; (b) 0.5 °C s^{-1}; (c) 2 °C s^{-1}; (d) 5 °C s^{-1}; (e) 10 °C s^{-1}; (f) 20 °C s^{-1}; (g) 30 °C s^{-1}; (h) 40 °C s^{-1}.

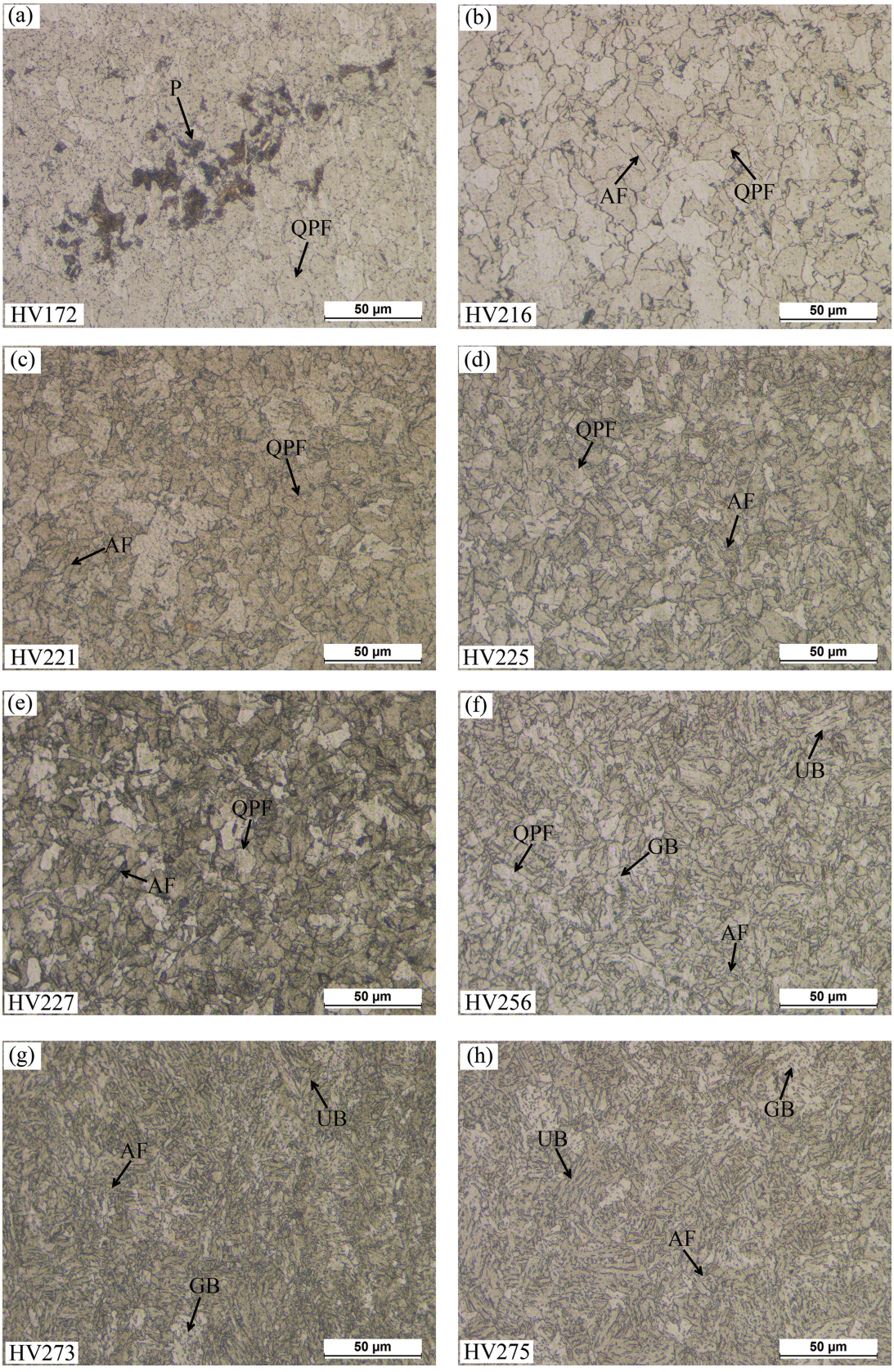

Figure 3: Optical microstructure of specimens at different cooling rates (1050 °C deformation): (a) 0.1 °C s^{-1}; (b) 0.5 °C s^{-1}; (c) 2 °C s^{-1}; (d) 5 °C s^{-1}; (e) 10 °C s^{-1}; (f) 20 °C s^{-1}; (g) 30 °C s^{-1}; (h) 40 °C s^{-1}.

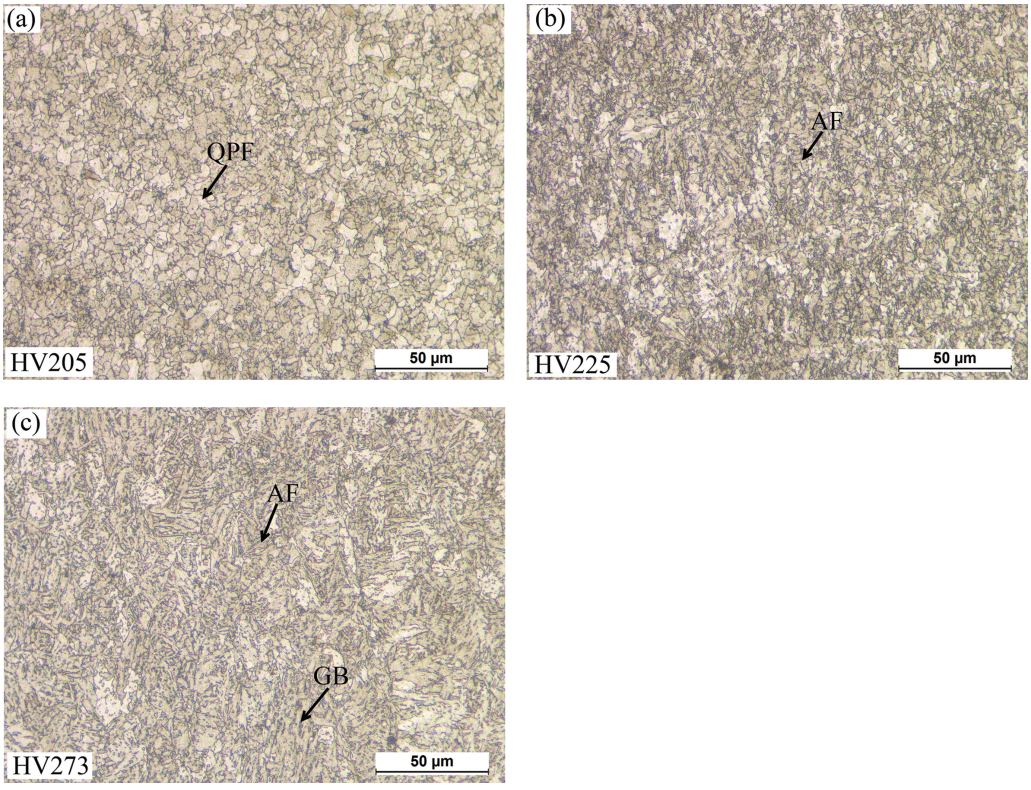

Figure 4: Optical microstructure of specimens at different cooling rates (900 °C deformation): (a) 2 °C s^{-1}; (b) 10 °C s^{-1}; (c) 40 °C s^{-1}.

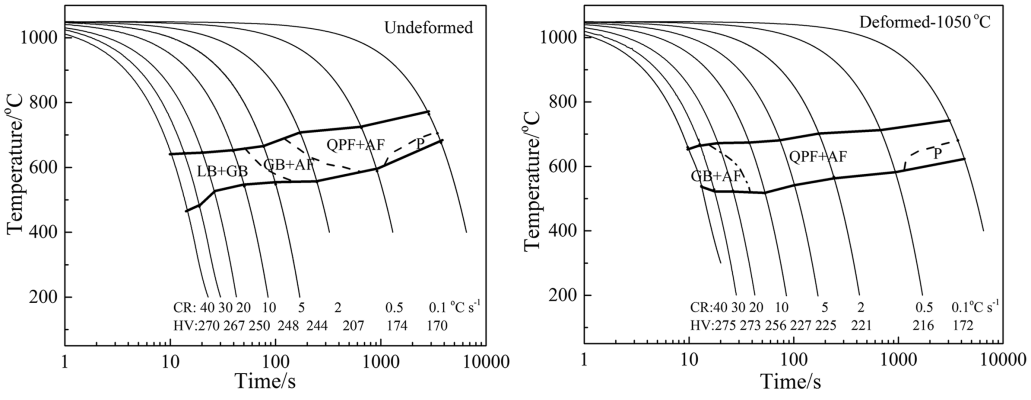

Figure 5: Continuous cooling transformation curves of steel (CCT diagram): (a) Static CCT; (b) Dynamic CCT.

measured from dilatometric data, and dash lines were determined by metallographic observations of OM and corresponding microhardness.

As shown in Figure 5, it could be found that the major transformation curves lie in the temperature ranges from 450 to 750°C in both static and dynamic CCT diagrams. Moreover, in comparison with the static CCT curve, the dynamic CCT curve moved toward the left side, proving that the AF and QPF areas were enlarged. LB microstructure could be obtained at cooling rate of 30°C s^{-1} in the static CCT curve, but that could not be observed at cooling rate of 40°C s^{-1} in the dynamic CCT curve. These results were consistent with the results of effects of deformation on microstructure transformation reported by Jun [11]. In conclusion, deformation could promote the formation of P and QPF in low-carbon HSLA steels.

It is well known that the CCT behavior and the corresponding transformed microstructure are related to prior hot deformation. Figure 6 showed Ar_3 and Ar_1 temperature

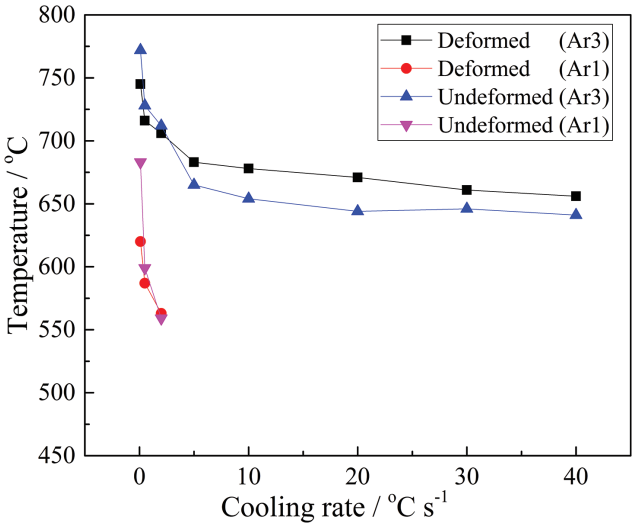

Figure 6: Ar_3 and Ar_1 temperature of specimens in undeformed and deformed conditions at different cooling rates.

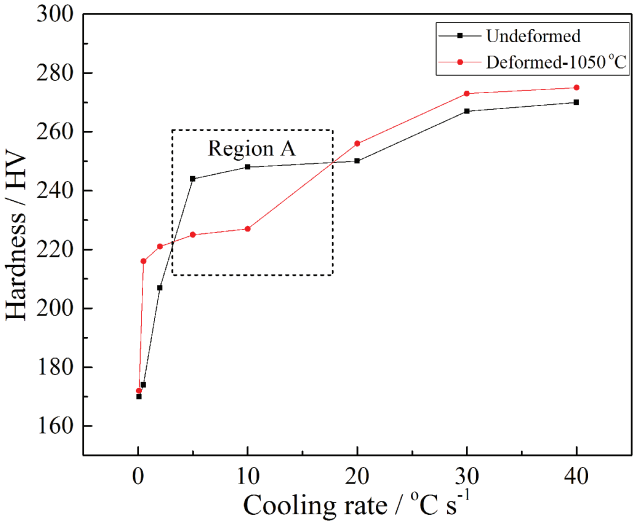

Figure 7: Hardness of specimens in undeformed and deformed conditions at different cooling rates.

of steels in undeformed and deformed conditions at different cooling rates. It could be seen that the deformation effectively improved Ar_3 temperatures.

Grain boundary surface areas per unit volume of austenite (Sv) and nucleation rate (Ns) were increased by austenite grain refinement and deformation below the temperature of non-recrystallization [12]. And that was expected to accelerate the AF and bainite formation and raise Ar_3 temperature as reported by other groups [13–15]. Liu and Solberg [16] results showed that the influence of deformation on the Ar_3 temperature decreases with decreasing cooling rate due to static recovery in the deformed austenite during cooling, which agreed with the results in Figure 6. Liang et al. [4] and Cizek et al. [17] indicated that the starting temperature of the bainite transformation was raised when applying deformation, this result was consistent with the observations made in the current studied steel. In conclusion, hot deformation increased transformation start temperature and promoted the formation of QPF and AF.

The hardness of specimens in undeformed and deformed condition at different cooling rates is shown in Figure 7. Figure 7 showed that hardness of specimens with deformation at 1,050°C was lower than that with undeformation in region A, which due to the hardness of microstructure composed of AF and QPF was lower than that consisted of UB and GB. Deformation in crystallization region could lead to the finer grain and higher hardness compared with undeformed condition at different cooling rates in addition to the ranges of region A.

Effects of hot deformation and deformed temperature on microstructure transformation

In order to investigate the effects of hot deformation and deformed temperature on microstructure transformation, the SEM micrographs of specimens at the cooling rate of 2, 10 and 40°C s^{-1} in Figures 2–4 are shown in Figure 8, respectively.

Figure 8 showed that microstructures with deformation at a temperature of 1,050and 900°C were markedly different from those without deformation. In the microstructure of specimens with deformation at temperature 1,050°C, the grain sizes of QPF and AF decreased and corresponding M/A islands became finer and disperse. In addition, in the microstructure of specimens with deformation at temperature 900°C, the oriented M/A islands and the prior austenite grain boundary networks were essentially eliminated. Meanwhile, the grains were distributed in a random manner. The above phenomenon could be explained as follows. When the specimens were deformed at temperature 1,050°C, austenite recrystallization led to the finer grain and small M/A islands. In addition, when the specimens were deformed at temperature 900°C, high densities of substructure and dislocation could be formed in the austenite, which increased the nucleation sites of AF, impeded the growth of the coherent and/or semicoherent γ/α interface and accelerated diffusion of carbon to the γ/α interface. At the same time, if the carbon contents of austenite near the γ/α interface were relatively decreased under deformation

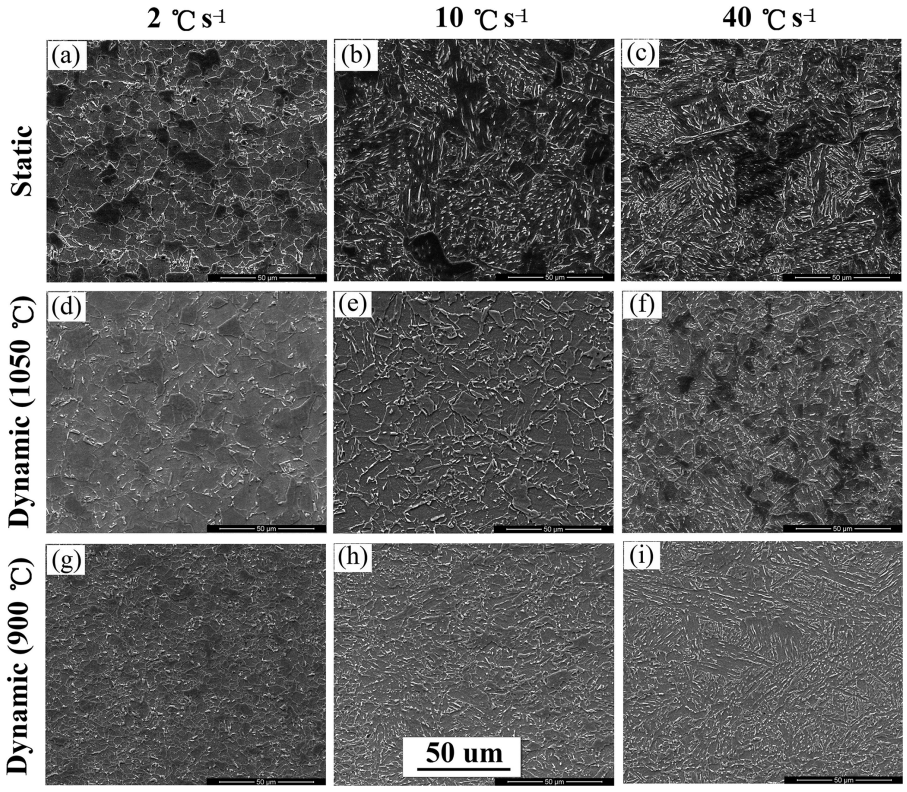

Figure 8: SEM micrographs of specimens at the cooling rate of 2, 10 and 40 ℃ s^{-1} in Figure 2, Figue 3 and Figure 4, respectively.

conditions, the corresponding M/A islands sizes could be decreased and the degree of dispersion could be increased.

Liang *et al.* [4] have attempted to discuss the thermodynamics and kinetics of the transformation of bainite in low-carbon steels. It can be concluded that nucleation rate played an important role in the morphology of ferrite and bainite in low-carbon steel. And nucleation rate was dependent on the driving force, which was mostly related to two factors: the transformation temperature and the cooling rate.

Deformation at 1,050°C resulted in complete recrystallization of the austenite, usually accompanied by grain refinement. And deformation at 900°C led to pancaked austenite grain shapes and an increase in the effective grain boundary area (surface areas per unit volume of austenite, Sv). As analyzed above all, deformed austenite increased Sv and, therefore, produced more nucleation sites for the formation of ferrite and bainite. Supposing the Gibbs free energy of original austenite was G_γ; and after deformation, the stored strain energy was defined as ΔG_d; and the volume-free energy was defined as ΔG_v. Then, the driving force for ferrite formation could be as shown in eqs. (3) and (4):

$$\Delta G_v = G_\alpha - G_\gamma, \text{undeformed austenite} \tag{3}$$

$$\Delta G_v^d = G_\alpha + \Delta G_d - G_\gamma, \text{deformed austenite} \tag{4}$$

Upon comparing the two eqs. (3) and (4), it can be seen that the driving force for ferrite transformation was higher for the deformed austenite, which increased the nucleation sites of AF and promotes the AF transformation.

With the combined consideration of ferrite and bainite transformed from austenite with and without deformation, it could be concluded that the size and morphology of ferrite and bainite were closely related to the controlled cooling rates. And a schematic diagram of Gibbs free energy changes for ferrite transformed from austenite is shown in Figure 9. In particular, T_0 was the temperature at which the two phases (austenite and ferrite) have the same energy. ΔT was signed as an undercooling degree (where $\Delta T = T_0 - T$, where T was the undercooling temperature).

It can be obtained that the deformation in austenite would increase the free energy of austenite (ΔG_d) compared to austenite without deformation at the same undercooling degree (ΔT). And it was also known that a large undercooling degree ΔT could cause a high nucleation rate, which resulted in the smaller size of ferrite or bainite microstructure accompanied with M/A.

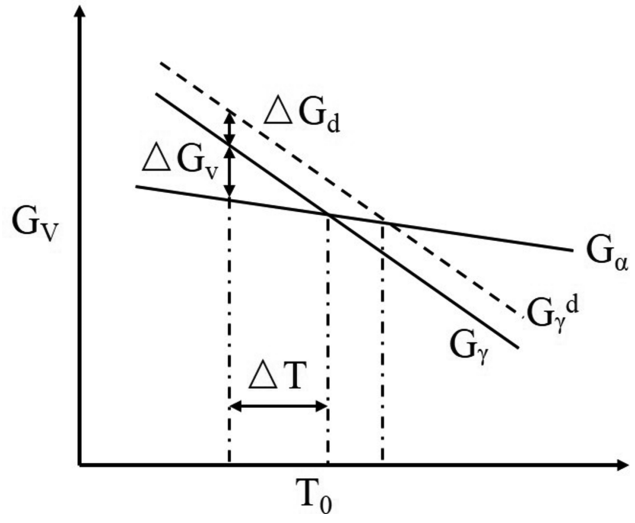

Figure 9: Schematic diagram of free energy changes for ferrite transformed from austenite.

Conclusion

(1) The microstructure formed in static and dynamic CCT was pearlite, QPF, AF, GB, UB and the accompanying martensite/austenite constitute (M/A island) depending on cooling rate and transformation temperature. In addition, LB was also formed in static CCT.

(2) The transformation curves of AF and GB moved toward to the left in dynamic CCT in comparison with the static CCT, which indicated that deformation promotes the formation of QPF and AF. Hence, the AF transformation area was enlarged and LB was not formed in dynamic CCT.

(3) As analyzed by thermodynamics and kinetics, finer bainite and the accompanying M/A could be obtained by reducing the bainite nucleation activation energy barrier as follows: (i) increasing the undercooling by increasing the cooling rate; (ii) increasing the stored energy by deformation of the austenite.

Acknowledgments: This work was financially supported by the Project of High-tech Ships of Ministry of Industry and Information Technology of the Peoples Republic of China (Grant Nos. [2014] 508).

References

[1] C.S. Lee, S. Kim, I.S. Suh, K.K. Um and O. Kwon, *J. Iron. Steel. Res. Int.*, 18 (2011) 796–802.
[2] X.W. Kong and C.L. Qiu, *J. Mater. Sci. Technol.*, 29 (2013) 446–450.
[3] D.S. Liu, Q.L. Li and T. Emi, Metall. Mater. Trans. A, 42 (2011) 1349–1361.
[4] X.J. Liang and A.J. Deardo, Metall. Mater. Trans. A, 45 (2014) 5173–5184.
[5] M.C. Zhao, K. Yang, F.R. Xiao and Y.Y. Shan, Metall. Mater. Sci. Eng., A, 335 (2003) 126–136.
[6] J. Hu, L.X. Du, J.J. Wang, H. Xie, C.R. Gao and R.D.K. Misra, Metall. Mater. Sci. Eng., A, 585 (2013) 197–204.
[7] Y.Q. Zhang, H.Q. Zhang, W.M. Liu and H. Hou, Mater. Sci. Eng., A, 499 (2009) 182–186.
[8] A.E. Amer, M.Y. Koo, K.H. Lee, S.H. Kim and S.H. Hong, *J. Mater. Sci.*, 45 (2010) 1248–1254.
[9] L.Y. Lan, C.L. Qiu, D.W. Z, X.H. Gao and L.X. Du, *J. Mater. Sci.*, 47 (2012) 4732–4742.
[10] B. Dutta and E.J. Palmiere, Metall. Mater. Trans. A, 34 (2003) 1237–1247.
[11] H.J. Jun, J.S. Kang, D.H. Seo, K.B. Kang and C.G. Park, Mater. Sci. Eng., A, 422 (2006) 157–162.
[12] H. Zhao, B.P. Wynne and E.J. Palmiere, *Mater. Charact.*, 123 (2017) 128–136.
[13] D.S. Liu, B.G. Cheng and Y.Y. Chen, Metall. Mater. Trans. A, 44 (2013) 440–455.
[14] D.S. Liu, B.G. Cheng and M. Luo, *ISIJ Int.*, 51 (2011) 603–611.
[15] N. Ishikawa, M. Okatsu, J. Shimamura, S. Endo, N. Shikanai, J. Kondo, R. Muraoka, Proceedings of the 26th International Conference on Offshore Mechanics and Arctic Engineering, OMAE2007, June 10–15, 2007, Ocean, Offshore and Arctic Engineering Division, San Diego, California, USA, pp. 185–191.
[16] X.D. Liu, J.K. Solberg and R. Gjengedal, Mater. Sci. Eng., A, 194 (1995) L15–L18.
[17] P. Cizek, B.P. Wynne, C.H.J. Davies, B.C. Muddle and P.D. Hodgson, Metall. Mater. Trans. A, 33 (2002) 1331–1349.